JOURNAL OF AIRCRAFT
Vol. 33, No. 1, January–February 1996

Separated Flow Mechanisms in F-18 Wing Rock

Lars E. Ericsson*
Mountain View, California 94040

In tests of the F/A-18 aircraft, wing rock was observed in laminar subscale tests as well as in full-scale flight, whereas wind-tunnel tests at an intermediate Reynolds number showed no wing rock. An analysis previously performed for a generic aircraft model was extended to identify the flow mechanisms behind this chain of events.

Nomenclature

b = wingspan
d = maximum body diameter
d_N = maximum nose diameter
L' = sectional lift, coefficient $c_l = L'/q_\infty(\pi d^2/4)$
L_N = nose length
l = rolling moment, coefficient $C_l = l/q_\infty Sb$
p = body roll rate
q_∞ = freestream dynamic pressure, $\rho_\infty U_\infty^2/2$
Re = Reynolds number based on maximum body diameter
S = reference area, projected wing area
t = time
U_∞ = freestream velocity
U_W = moving wall velocity
x = axial body coordinate
α = angle of attack
β = angle of sideslip
Δ = increment and amplitude
Δt = time lag
θ_A = apex half-angle
ϕ = roll angle

Subscripts
dyn = dynamic
st = static
1, 2, 3 = numbering subscripts
∞ = freestream conditions

Introduction

THIS article extends an earlier analysis of the roll-induced coupling between forebody and LEX vortices.[1,2] Flight tests of the F-18 HARV show a buildup of the wing rock towards and possibly past 30 deg[3] (Fig. 1). Some insight into the flow physics of this wing rock was provided by a film clip shown by Nelson.[4] Both the full-scale flow visualization and the one with a small model in a wind tunnel at $Re < 0.02 \times 10^6$ or 20,000 showed a very extensive interaction between forebody and leading-edge-extension (LEX) vortices,[4,5] resulting in large amplitude wing rock (Fig. 2). When comparing flight data with wind-tunnel measurements, one has to account for the bearing friction present in the wind-tunnel test. It has been observed to have a very significant effect on the wing-rock boundary for an 80-deg delta wing.[6] The predicted boundary for free flight[7] shows wing rock to start at $\alpha \approx 20$ deg. In a wind-tunnel test with a regular bearing,[8] wing rock started at $\alpha \approx 27$ deg. However, when the same air bearing was used as in the F/A-18 test,[5] wing rock started already at $\alpha \approx 22$ deg (Ref. 9), only 2 deg later than what was predicted for free flight.[6,7] Assuming that the bearing friction has a similar effect on the present wing-rock results, one obtains the data trend shown by a dashed line in Fig. 2. The agreement with the flight test results is still amazingly good. When testing a larger F-18 model in a wind tunnel at NASA Langley Research Center, at a much higher Reynolds number than in the Notre Dame tunnel test, Nguyen et al.[10] did not observe any wing rock at all. This illustrates the difficulties discussed in Ref. 11. The situation is the opposite of that encountered earlier in tests of a generic aircraft model.[12] In this case, tests at NASA Langley (in the same tunnel and at a similar Reynolds number) showed wing rock to exist,[12] whereas it would not occur in laminar flow[13,14] and would be less severe at full-scale Reynolds numbers.[15] This article presents a separated-flow hypothesis that can explain these contradictory experimental results.

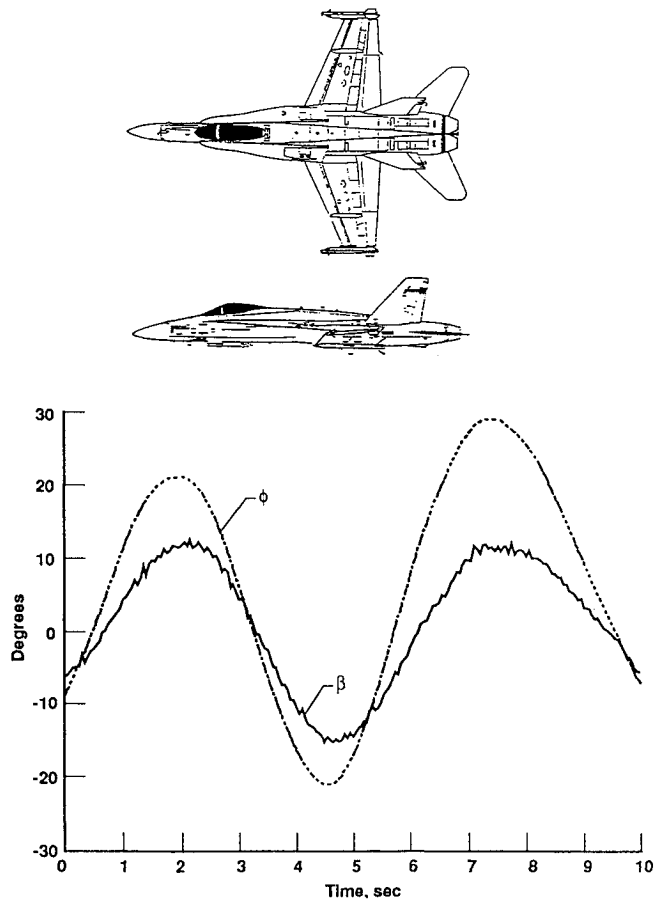

Fig. 1 Wing-rock buildup of the F-18 HARV aircraft.[3]

Received Jan. 17, 1995; revision received June 21, 1995; accepted for publication July 14, 1995.

*Engineering Consultant. Fellow AIAA.

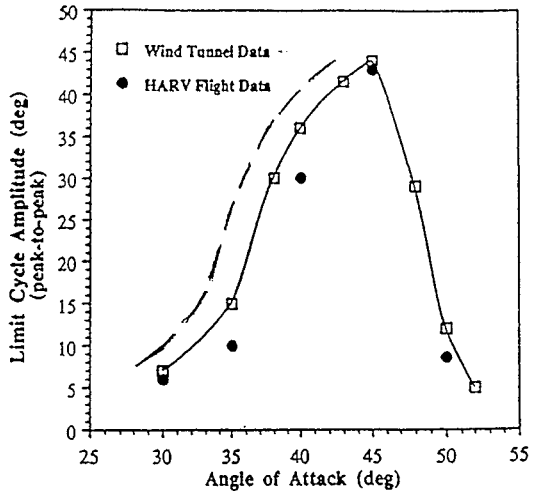

Fig. 2 Measured wing-rock amplitude of the F/A-18 aircraft.[5]

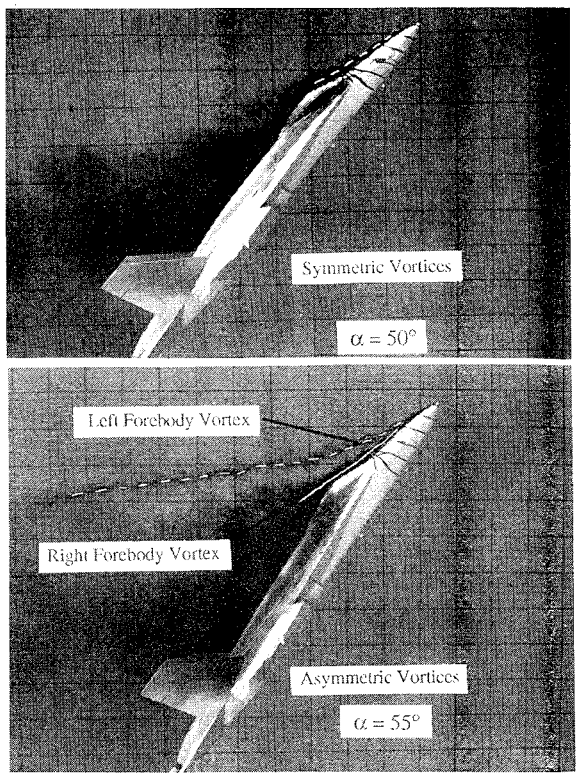

Fig. 3 F/A-18 forebody flow visualization at α = 50 and 55 deg.[16]

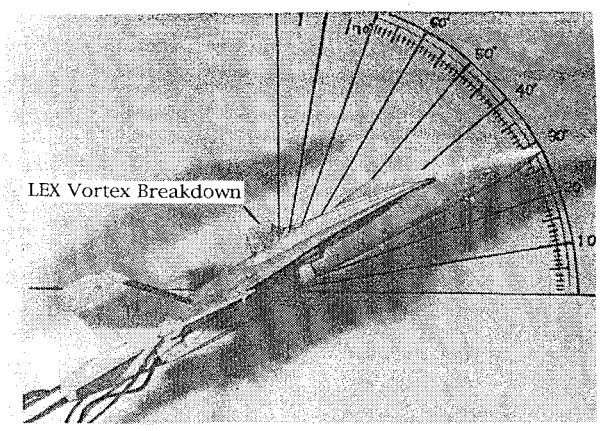

Fig. 4 Observed LEX–vortex breakdown in static test at α = 29 deg.[18]

Analysis

The high-alpha forebody flow on a model of F/A-18 was investigated in conjunction with a water-tunnel test of forebody blowing.[16] The flow visualization for no blowing shows that the forebody vortices are symmetric at α = 50 deg, but become asymmetric at α = 55 deg, with the lower of the vortices, the one that is not lifted-off, staying close to the nose contour (Fig. 3). In another test,[17,18] flow visualization showed spiral breakdown of the LEX vortex (Fig. 4).

Based upon the flow photographs in Figs. 3 and 4, one can construct the conceptual forebody–LEX vortex geometry shown in Fig. 5 to explain the interaction described by Nelson's film clip.[4] It showed how one of the forebody vortices at a high angle of attack would dip down to interact with the LEX vortex on that side of the body. That started the wing-rocking action, with the forebody–LEX vortex interaction alternating between the two sides. Section A-A in Fig. 5 illustrates how the LEX vortex, after spiral vortex breakdown, would generate a velocity field that drags down the forebody vortex, starting a spiraling interaction by the two vortices. The good agreement in Fig. 2 between flight data and one degree-of-freedom free-to-roll test results in a wind tunnel indicates that the yaw degree of freedom in flight (Fig. 1) did not change the character of the wing rock in any fundamental way. Consequently, only the roll degree of freedom will be considered in the analysis to follow.

It was suggested in Refs. 1 and 2 that the vortex interaction caused the beneficial effect of the LEX vortex on the loading of the adjacent wing to be lost or greatly decreased. This would increase the magnitude of the statically stabilizing roll-

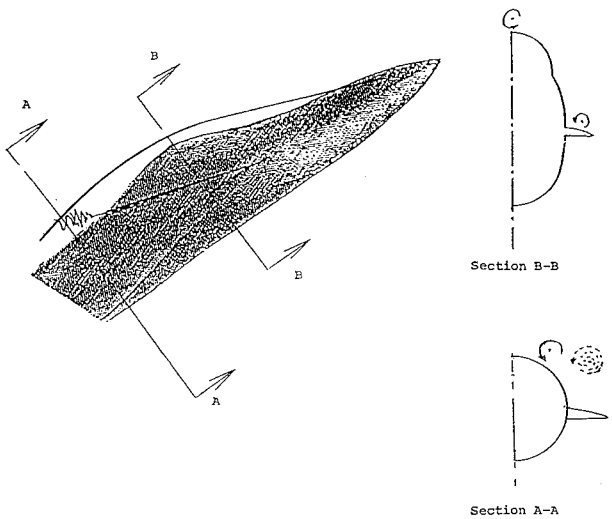

Fig. 5 Conceptual flow geometry for LEX–forebody vortex interaction.

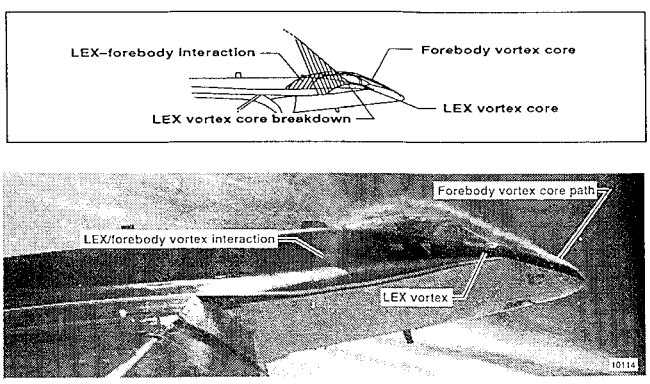

α = 40.6° and β = 0.6°.

Fig. 6 LEX–forebody vortex interaction in flight.[20]

ing moment and, through the effect of convective flow time lag, would cause a loss of roll damping, resulting in the observed wing rock. Flight test results[19,20] show that such an interaction indeed takes place (Fig. 6).

Moving Wall Effects

Moving wall effects[21] generate wing rock through their influence on the forebody crossflow separation and associated vortex shedding.[13,14] They are very dependent upon the crossflow Reynolds number in regard to the nature of their induced aerodynamic effects. This is illustrated by Magnus lift measurements on a rotating circular cylinder[22] (Fig. 7). For laminar flow conditions (curve f in Fig. 7a for $U_W/U_\infty < 0.3$), positive Magnus lift is generated. This is mainly the result of the separation delay on the top side through the downstream moving wall effects. In contrast, at critical flow conditions, negative Magnus lift is generated by the promotion of transition on the bottom side through upstream moving wall effects, causing a change from the subcritical to the supercritical type of flow separation, e.g., at $Re = 0.128 \times 10^6$ and $U_W/U_\infty \geq 0.3$ (curve f in Fig. 7a). The negative Magnus lift reaches its maximum magnitude when the crossflow conditions are of the critical type already in the static case (curves j, k, and l in Fig. 7a). In the turbulent, supercritical case (curve n in Fig. 7b for $U_W/U_\infty < 0.1$), the main effect is that of the upstream moving wall effect on the bottom side, which promotes flow separation, moving it from the supercritical towards the subcritical position. Thus, the difference in Magnus lift between laminar and turbulent flow conditions is mainly the result of the difference between the capability of the moving wall effect to delay laminar flow separation and promote turbulent separation. The difference in Magnus lift slopes, the laminar one (Fig. 7a) being only three-eighths of the turbulent one (Fig. 7b), reflects the fact that it is much more difficult to delay than to promote flow separation.

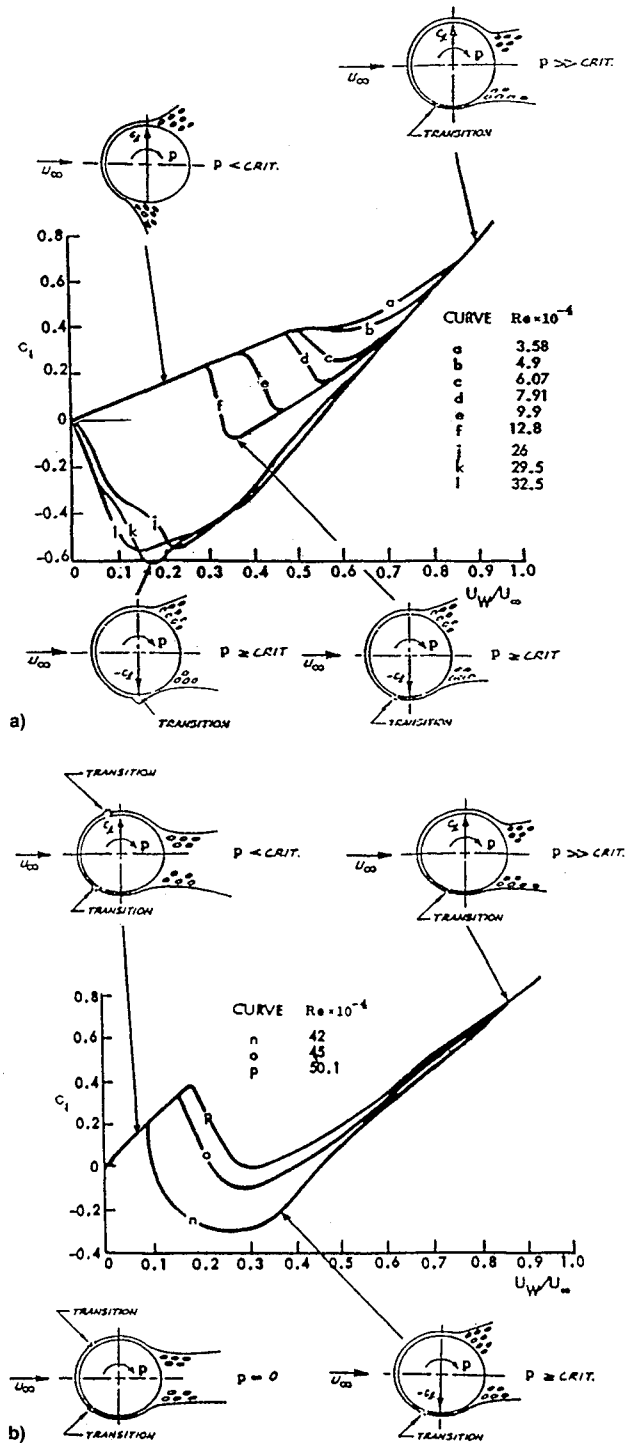

Fig. 7 Magnus lift characteristics for a rotating circular cylinder[22]: a) initially subcritical (laminar) and b) initially supercritical (turbulent) flow conditions.

The Reynolds number based upon the maximum forebody diameter of the generic aircraft model was $Re = 0.26 \times 10^6$ in the test,[12] and therefore, in all likelihood in the critical Re regime[22] (Fig. 7a). Thus, the crossflow over the nose and nose shoulder was in the critical Re region, and the scenario in Fig. 8 can be visualized. At $t = t_1$, the adverse upstream moving wall effect on the forebody crossflow causes boundary-layer transition to occur earlier, as illustrated in the figure. The effect is similar to that of changing the separation from the subcritical to the critical or supercritical type (Fig. 7a). In the absence of time lag effects, the vortex geometry sketched at $t = t_1$ would result. Because of time lag effects similar to those for slender wing rock,[23] this vortex geometry is not realized until $t = t_2 = t_1 + \Delta t$. For simplicity, only the vortex closest to the body is shown at t_2, as it indicates the direction of the vortex-induced downwash on the wing and the resulting rolling moment. At $t = t_3$, when the roll rate reaches its maximum in the opposite direction, another forebody switch of the flow separation asymmetry occurs. Because of the time lag effect, the vortex geometry influencing the now horizontal wing has not changed, but is the same as at $t_2 = t_1 + \Delta t$, in agreement with the flow pictures in Ref. 12. During Δt, required for the new vortex geometry to reach the wing, the vortex-induced rolling moment generated by the previous vortex geometry drives the rolling motion.[13,14] This is the mechanism generating the observed wing rock.[12]

F-18 Wing Rock

Using the information in Figs. 3–6, the flow sketch corresponding to Fig. 8 looks for the subscale test of the F/A-18 model as shown in Fig. 9. The downstream moving wall effect delays flow separation for laminar flow conditions ($U_W/U_\infty <$ 0.3 for curve f in Fig. 7a). In Fig. 9 the aerodynamic spring needed for the oscillatory wing-rock motion is provided by the rolling moment generated by the loss of lift on the main wing through the vortex interaction. As in the case of the generic aircraft model in Fig. 8, there is a time lag Δt after the rotation of the forebody has changed before the vortex interaction occurs. This generates the rolling moment that drives the wing-rock motion, just as in the case of the generic wing rock in Fig. 8. The time lag effect is well illustrated by flight-test results[19] (Fig. 10). The maximum roll rate at $\phi =$ 0 generates the delay of crossflow separation causing the lowering of the forebody vortex sketched in Fig. 5. Because of the time lag effect the resulting lowering of the vortex at the LEX occurs at $t_2 = t_1 + \Delta t$ (Fig. 9). This is in good agreement with what the frames in Fig. 10 show. The shown vortex location was observed by the pilot, seated above the LEX.

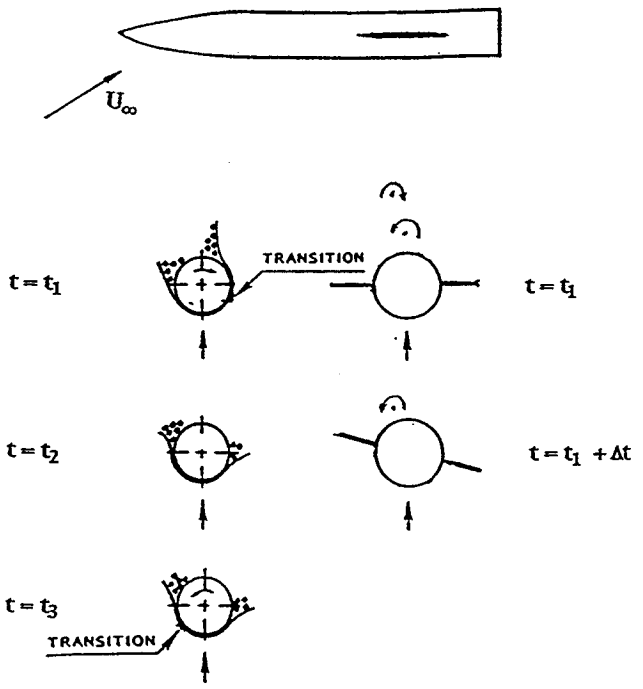

Fig. 8 Conceptual flow mechanism for forebody-induced wing rock of a generic aircraft model.[13]

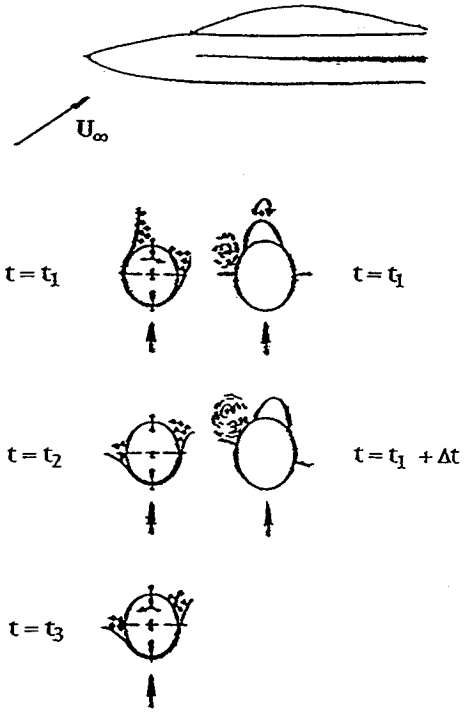

Fig. 9 Conceptual flow mechanism for LEX-forebody vortex interaction.

The wing-rock amplitude of F/A-18, observed in flight and measured at low Reynolds numbers in wind-tunnel tests,[5] shows the amplitude to increase with angle of attack, from approximately 3 deg at $\alpha = 30$ deg to a maximum of slightly more than 20 deg at $\alpha = 45$ deg (Fig. 2). When the angle of attack is increased further, the limit cycle amplitude decreases rapidly. The reasons for these data trends will be discussed next. From Figs. 3 and 4 one obtains $l_N/d_N \approx 2.5$. For a tangent–ogive nose the corresponding apex half angle would be $\theta_A \approx 24$ deg, indicating that static asymmetric forebody vortices should start developing when $\alpha > 2\theta_A = 48$ deg.[24]

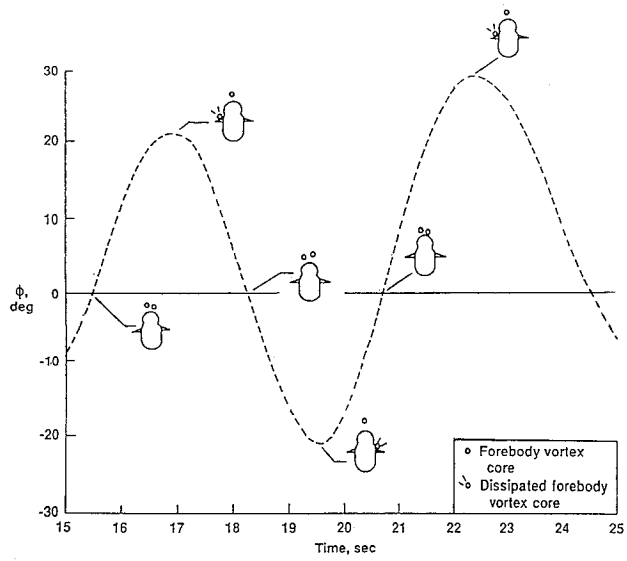

Fig. 10 Forebody vortex location on rolling F-18 flight vehicle.[19]

This is in good agreement with the flow visualization results in Fig. 3, showing that asymmetric forebody vortices started occurring at $\alpha > 50$ deg. It is also in agreement with the measured yawing moment at zero sideslip.[3] As discussed in Ref. 25 in connection with test results for a spinning nose tip,[26] the moving wall effect is largest just before natural separation asymmetry occurs at $\alpha \geq 50$ deg. At that point, the symmetric flow separation is easiest to perturb to change the symmetric vortex pattern to an asymmetric one in the direction dictated by the moving wall effect.

The rapid decline of the wing-rock amplitude at higher angles of attack[5] (Fig. 2) reflects the fact that the moving wall effect now has to overcome the natural, static separation asymmetry. The observant reader probably is questioning why the peak amplitude in Fig. 2 occurs at $\alpha \approx 45$ deg, when experimental results show static flow asymmetry to occur at $\alpha > 50$ deg. The likely reason for this is that, within a certain α-range below that at which static flow asymmetry develops, even a moving wall effect of modest magnitude will cause the symmetric flow separation to become asymmetric. Once it is asymmetric it will take a moving wall effect of significant magnitude to reverse the separation asymmetry. This is in agreement with the experienced difficulty in developing reliable means for control of the crossflow asymmetry on a slender nose.[27] The data trend for $\alpha < 45$ deg in Fig. 2 is the expected one. Farther and farther away from the trigger point $\alpha \approx 50$ deg the moving wall effect will have more and more difficulty in trying to perturb the symmetric flow separation.

The agreement between the wind-tunnel test and free-flight results in Fig. 2 appears at first rather surprising. It is well known[24] that static side forces generated by asymmetric forebody flow separation are of similar magnitudes for laminar and turbulent flow. However, one must also compare the laminar and turbulent moving wall effects. Figure 7 shows the Magnus lift measured by Swanson[22] on a rotating circular cylinder. In the laminar, subcritical case (Fig. 7a), the Magnus lift is generated mainly by the downstream moving wall effect on the top side, which moves the flow separation from the subcritical towards the supercritical position. In the turbulent, supercritical case (Fig. 7b), the Magnus lift is generated mainly by the adverse, upstream moving wall effect on the bottom side, which moves the flow separation forward from the supercritical towards the subcritical position.

In the present case of interest the laminar flow separation is delayed by the moving wall effect from the static position S_{st} to the dynamic position S_{dyn} (Fig. 11a), whereas the tur-

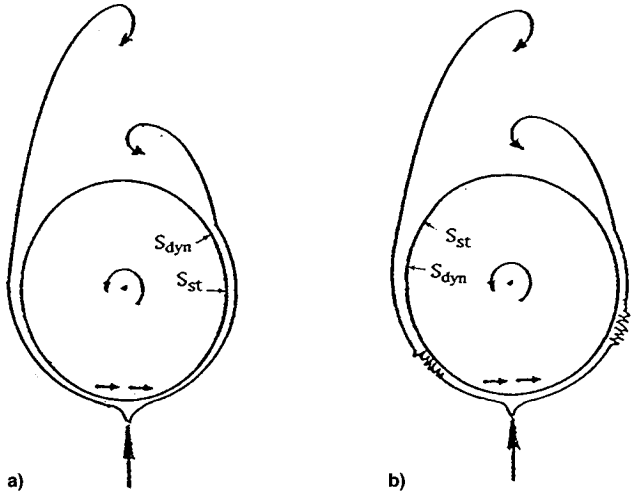

Fig. 11 Conceptual roll-induced asymmetric forebody vortex geometries: a) laminar and b) turbulent crossflows.

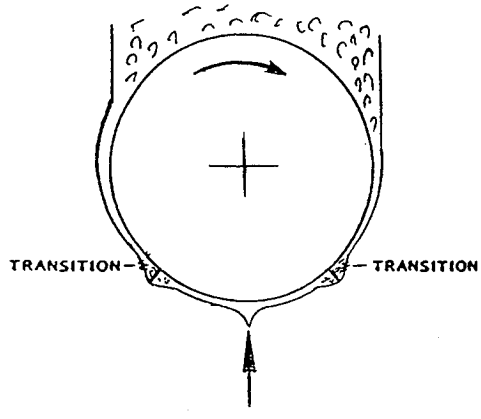

Fig. 12 Flow sketch of conceptual effect of body strakes on forebody crossflow at critical flow conditions.

bulent separation is promoted (Fig. 11b). The result is a forebody vortex pair that looks very similar.

Reynolds Number Effects

Based upon the results in Figs. 7 and 8, one expects the effect of rotation on the flow separation and associated vortex geometry to switch if the laminar Reynolds number is increased to fall in the critical range. There, the moving wall effect does not influence the flow separation directly, as in the cases illustrated in Figs. 9–11, but acts instead only indirectly through its effect on boundary-layer transition, as illustrated in Fig. 7a and discussed in connection with Fig. 8. This reverses the ultimate moving wall effect on crossflow separation. Thus, the forebody–LEX vortex interaction would become statically destabilizing/dynamically stabilizing, and no wing rock should occur. That is exactly what was observed when the F/A-18 model was tested[10] at roughly the same crossflow Reynolds number, $Re \approx 0.26 \times 10^6$, for the forebody as in the case of the generic aircraft model.[12] However, when the forebody of the F/A-18 model was provided with small strakes, at ±40-deg azimuth from the bottom meridian, wing rock did occur.[10] The logical reason for this is that the strakes caused early, localized, transitional flow separation with turbulent reattachment, resulting in final, turbulent flow separation, with moving wall effects similar to those for laminar flow (Fig. 12). A similar supercritical type of flow separation would probably also result if the strakes were substituted by boundary-layer trips,[24] preferably placed farther away from the flow stagnation point than the strakes in Fig. 12.

These results illustrate the fact that dynamic simulation of separation-induced self-excited oscillations in subscale tests is not possible unless the full-scale Reynolds number is simulated.[11] One encouraging result of the present analysis is that it indicates that, even in the presence of so-called moving wall effects, analytic extrapolation to full-scale vehicle dynamics from subscale tests may be possible, provided that the fluid mechanics involved are fully understood.

Conclusions

A brief analysis of recent experimental results for the F/A-18 aircraft has led to the following conclusions:

1) The wing rock of the F/A-18 aircraft can be explained by extending the analysis performed earlier for the wing rock of a generic aircraft model.

2) The main change is that instead of inducing downwash on the main wing, the forebody vortex in the present case interacts with the LEX vortex, controlling its lift generating effect on the main wing.

3) It needs to be emphasized that in the present case the roll-induced moving wall effect acts directly on the crossflow separation, delaying it for both laminar and turbulent flow conditions, whereas in the case of the generic aircraft experiment, the moving wall effect controlled the crossflow separation via its effect on boundary-layer transition.

Acknowledgments

This article is, in part, based upon results from the initial phase of a study being performed for Advanced Research Projects Agency, Contract DAAH01-94-C-R022, under the direction of M. S. Francis. The author wishes to thank M. E. Beyers, Institute for Aerospace Research, National Research Council, Canada, for many helpful discussions.

References

[1]Ericsson, L. E., "Dynamic LEX/Forebody Vortex Interaction Effects," AIAA Paper 92-2732, June 1992.

[2]Ericsson, L. E., "F-18 Wing Rock Considerations," International Council of the Aeronautical Sciences, ICAS Paper 94-3.4.2, Sept. 1994.

[3]Fisher, D. F., and Cobleigh, B. R., "Controlling Forebody Asymmetries in Flight-Experience with Boundary Layer Transition Strips," AIAA Paper 94-1826, June 1994.

[4]Nelson, R. C., "Unsteady Aerodynamics of Slender Wings," AGARD-R-776, April 1991 (Paper 1).

[5]Quast, T., Nelson, R. C., and Fisher, D. F., "A Study of High-Alpha Dynamics and Flow Visualization for a 2.5% Model of the F-18 HARV Undergoing Wing Rock," AIAA Paper 91-3267, Sept. 1991.

[6]Ericsson, L. E., "Slender Wing Rock Revisited," *Journal of Aircraft*, Vol. 30, No. 3, 1993, pp. 352–356.

[7]Ericsson, L. E., and King, H. H. C., "Rapid Prediction of High-Alpha Unsteady Aerodynamics of Slender-Wing Aircraft," *Journal of Aircraft*, Vol. 29, No. 1, 1992, pp. 85–92.

[8]Nguyen, L. T., Yip, L. P., and Chambers, J. R., "Self-Induced Wing Rock of Slender Delta Wings," AIAA Paper 81-1883, Aug. 1981.

[9]Arena, H. S., Jr., Nelson, R. C., and Schiff, L. B., "An Experimental Study of the Nonlinear Dynamic Phenomenon Known as Wing Rock," AIAA Paper 90-2812, Aug. 1990.

[10]Nguyen, L. T., private communication, April 1991.

[11]Ericsson, L. E., "Effects of Transition on Wind Tunnel Simulation of Vehicle Dynamics," *Progress in Aerospace Sciences*, Vol. 27, No. 1, 1990, pp. 121–144.

[12]Brandon, J. M., and Nguyen, L. T., "Experimental Study of Effects of Forebody Geometry on High Angle of Attack Stability," *Journal of Aircraft*, Vol. 25, No. 7, 1988, pp. 591–597.

[13]Ericsson, L. E., "Wing Rock Generated by Forebody Vortices," *Journal of Aircraft*, Vol. 26, No. 2, 1989, pp. 110–116.

[14]Ericsson, L. E., and Mendenhall, M. R., "On Forebody-Induced Wing Rock," AIAA Paper 94-0167, Jan. 1994.

[15]Ericsson, L. E., "Prediction of High-Alpha Vehicle Dynamics," International Council of the Aeronautical Sciences, ICAS-90-3.6.1, Sept. 1990.

[16]Suárez, C. J., and Malcom, G. N., "Water Tunnel Force and Moment Measurements on an F/A-18," AIAA Paper 94-1802, June 1994.

[17]Hebbar, S. K., Platzer, M. F., and Cavazos, O. V., "A Water Tunnel Investigation of the Effects of Pitch Rate and Yaw on LEX Generated Vortices of an F/A-18 Fighter Aircraft Model," AIAA Paper 91-0280, Jan. 1991.

[18]Cavazos, O. V., Jr., "A Flow Visualization Study of LEX Generated Vortices on a Scale Model of a F/A-18 Fighter Aircraft at High Angles of Attack," M.S. Thesis, U.S. Naval Postgraduate School, Monterey, CA, June 1990.

[19]Fisher, D. F., DelFrate, J. H., and Richwine, D. M., "In-Flight Flow Visualization Characteristics of the NASA F-18 High Alpha Research Vehicle at High Angles of Attack," NASA TM 4193, May 1990.

[20]Fisher, D. F., DelFrate, J. H., and Zuniga, F. A., *Summary of In-Flight Flow Visualization Obtained from the NASA High Alpha Research Vehicle*, NASA CP 3149, Pt. I, Vol. 1, 1990, pp. 205–242; also NASA TM-101734, Paper 8, 1990.

[21]Ericsson, L. E., "Moving Wall Effects in Unsteady Flow," *Journal of Aircraft*, Vol. 25, No. 11, 1988, pp. 977–990.

[22]Swanson, W. M., "The Magnus Effect: A Summary of Investigations to Date," *Journal of Basic Engineering*, Vol. 83, No. 9, 1961, pp. 461–470.

[23]Ericsson, L. E., "The Fluid Mechanics of Slender Wing Rock," *Journal of Aircraft*, Vol. 21, No. 5, 1984, pp. 322–328.

[24]Ericsson, L. E., and Reding, J. P., "Asymmetric Flow Separation and Vortex Shedding on Bodies of Revolution," *Tactical Missile Aerodynamics: General Topics*, edited by M. J. Hemsch, Vol. 141, Progress in Astronautics and Aeronautics, AIAA, Washington, DC, 1992, pp. 391–452.

[25]Ericsson, L. E., "Unsteady Separation on Slender Bodies at High Angles of Attack," *Journal of Spacecraft and Rockets*, Vol. 30, No. 6, 1993, pp. 689–695.

[26]Fidler, J. E., "Active Control of Asymmetric Vortex Effects," *Journal of Aircraft*, Vol. 18, No. 4, 1981, pp. 267–272.

[27]Ericsson, L. E., "Control of Forebody Flow Asymmetry—A Critical Review," AIAA Paper 90-2883, Aug. 1990.